Title

Observation of Potential-Induced Hydration on the Surface of Ceramic Proton Conductors Using In Situ Near-Ambient Pressure X-ray Photoelectron Spectroscopy

Journal

The Journal of Physical Chemistry Letters, 13(13)

ISSN

1948-7185

Authors

Zhao, Zihan

Ling, Xiao

Gabaly, Farid El

et al.

Publication Date

2022-04-07

DOI

10.1021/acs.jpclett.2c00114

Observation of Potential-Induced Hydration on the Surface of Ceramic Proton Conductors Using *In Situ* Near-Ambient Pressure X-ray Photoelectron Spectroscopy

Zihan Zhao[a], Xiao Ling[a], Farid El Gabaly[b], Michael Grass[c], Naila Jabeen[c,d], Deborah Jones[e], Zhi Liu[c,f], Bongjin S. Mun[g], Artur Braun[,h,i], and Qianli Chen[*,a,h]*

AUTHOR ADDRESS

[a] University of Michigan - Shanghai Jiao Tong University Joint Institute, Shanghai Jiao Tong University, Shanghai 200240, China

[b] Sandia National Laboratories, Livermore, California 94551, US

[c] Advanced Light Source, Lawrence Berkeley National Laboratory, Berkeley, CA 94720, USA

[d] Nanoscience and Technology Division, National Center for Physics, Quaid-i-Azam University Campus, Islamabad 44000, Pakistan

[e] ICGM, Université Montpellier, CNRS, ENSCM, F-34095 Montpellier cedex 5, France

[f] Shanghai Institute of Microsystem and Information Technology, Chinese Academy of Sciences, Shanghai 200050, China

[g] Department of Physics and Photon Science, Gwangju Institute of Science and Technology, Buk-gu Gwangju 500-712, Korea

[h] Laboratory for High Performance Ceramics, Empa, Swiss Federal Laboratories for Materials Science and Technology, CH-8600 Dübendorf, Switzerland

[i] University of Hawai'i at Manoa, Hawai'i Natural Energy Institute, Honolulu, HI 96822, USA

AUTHOR INFORMATION

Corresponding Author

Qianli Chen – orcid.org/0000-0001-8460-0596; Email: qianli.chen@sjtu.edu.cn

Artur Braun – orcid.org/0000-0002-6992-7774; Email: Artur.Braun@alumni.ethz.ch

ABSTRACT

Interactions of ceramic proton conductors with the environment under operating condition play an essential role on material properties and device performance. It remains unclear how the chemical environment of material, as modulated by the operating condition, affects the proton conductivity. Combining near-ambient pressure X-ray photoelectron spectroscopy and impedance spectroscopy, we investigate the chemical environment changes of oxygen and the conductivity of $BaZr_{0.9}Y_{0.1}O_{3-\delta}$ under operating condition. Changes in O 1s core level spectra indicate that adding water vapor pressure increases both hydroxyl groups and active proton sites at undercoordinated oxygen. Applying external potential further promotes this hydration effect, in particular, by increasing the amount of undercoordinated oxygen. The enhanced hydration is

accompanied by improved proton conductivity. This work highlights the effects of undercoordinated oxygen for improving the proton conductivity in ceramics.

TOC GRAPHICS

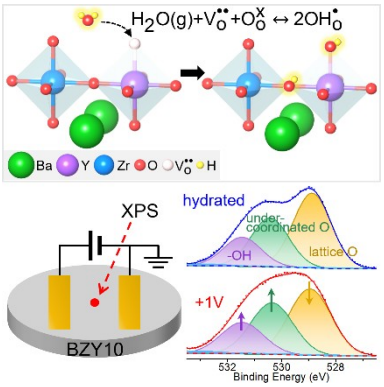

KEYWORDS: Proton conductivity, surface chemistry, *in situ* X-ray photoelectron spectroscopy, ceramic electrolyte, Y-doped barium zirconate

Ceramic proton conductors are promising solid electrolytes for intermediate temperature solid oxide fuel cells and electrolyzers.[1-3] Yttrium-doped $BaZrO_3$ is one of the well-studied ceramic proton conductors with high proton conductivity and stability.[4, 5] Substitutions of the tetravalent cations (Zr^{4+}) on the perovskite B site by trivalent cations (Y^{3+}) create oxygen vacancies ($V_O^{\cdot\cdot}$) to compensate the charge neutrality. Hydration occurs via dissociation of water by filling of these oxygen vacancies and forming hydroxide ions ($OH_O^{\cdot}$, or considered as hydroxyl protons), given by:[6, 7]

$$H_2O(g) + V_O^{\bullet\bullet} + O_O^x \Leftrightarrow 2OH_O^{\bullet}$$

The proton conduction mechanism is generally understood as proton hopping between adjacent oxygen sites via a Grotthuss mechanism.[8, 9] The performance of proton conductors is thus strongly influenced by the hydration process because of the formation of hydroxyl protons.[10, 11]

Many researchers have studied the effects of material structure and composition on proton transport in ceramics.[12-16] Investigating the surface chemistry between solid and ambient gas interface can lead to better understanding of the ion site activity,[17] proton and oxygen transport.[18-21] Encouraging results have established that in different environment, proton transport properties are strongly influenced by hydration-induced changes in surface chemistry.[22-25] Stub et al.[18] showed that different structures of the adsorbed water layer on oxide surface affect the activation energy for proton transport. To study the mechanism of surface hydration at relevant conditions, such as temperature and atmosphere, *in situ* spectroscopic probes are highly effective approaches.[26-28] In particular, *in situ* X-ray photoelectron spectroscopy (XPS) has provided inspiring results on proton conductors: our previous work[29] showed the $V_O^{\cdot\cdot}$ filling upon hydration is associated with charge redistribution between ions; Jarry et al.[30, 31] observed that surface composition affects OH^- formation at different conditions for $BaCe_xZr_{0.9-x}Y_{0.1}O_{2.95}$ thin films.

On the other hand, there have been intriguing discoveries that applying external potential to the proton ceramic electrolysis cells (PCECs) reduces the resistance of proton conducting electrolyte.[32-35] Gan et al.[33] and Li et al.[35] observed that applying potentials up to 2 V to PCECs can reduce both series resistance and electrode polarization resistance and improve current

efficiency. Chen et al.[32] explained the reduced resistance due to space-charge layer effect on electron charge transfer. However, it is unclear whether the applied potential induces chemical environment changes, which contribute to the reduced resistance. Hence, *in situ* spectroscopic measurements on ceramic proton conductors with applying working potential are necessary for further exploration of the underlying mechanisms.

In the present work, the interactions between $BaZr_{0.9}Y_{0.1}O_{3-\delta}$ (BZY) and humid environment are investigated using *in situ* near-ambient pressure XPS (NAP-XPS) under operating conditions, combined with proton conductivity measured by impedance spectroscopy. Water vapor pressure and external potential are applied to simulate the working environment in a PCEC. The chemical environment of oxygen on the surface during hydration and the corresponding proton conductivity are discussed.

Figure 1(a, b) shows the measurement setup of BZY pellet with two gold electrodes. Sample preparation and other details about equipment can be found in Supporting Information (SI). Prior to the measurement, the pellet was subjected to a dehydration procedure in ultra-high vacuum (UHV) chamber at about 800 K for 16 hours. After thermal treatment in the reductive condition of UHV, more oxygen vacancies $V_O^{\cdot\cdot}$ would form in the materials.[36, 37] The rising $V_O^{\cdot\cdot}$ concentration may benefit the hydration process and the formation of hydroxyl protons. The survey spectrum for BZY10 after dehydration procedure in UHV with photon energy of 490 eV is shown in Figure S1. Peaks from Ba, Y, Zr core level and the C impurity are presented.
Then, XPS and impedance spectra were recorded subsequently in UHV at about 550 K (denoted as “dry”), after introducing 200 mTorr water vapor (“hydrated”), and applying 1 V potential to the working electrode (WE) under hydrated condition (“hydrated +1V”). Since the standard

water splitting potential is 1.23 V and practically, 1.3 V or higher potential required in PCECs,[38, 39] water electrolysis was avoided in our measurement by applying potential of only 1 V. Hence, the impact of the external potential on barely the hydration process of BZY is investigated.

Figure 1(c) shows the O 1s core level XPS spectra of BZY under the three aforementioned conditions – from dry to hydrated, then to hydrated +1V, recorded with photon energy of 700 eV (original spectra shown in Figure S2). As shown in Figure S2, the as measured O 1s spectra have clear offset for the case of "hydrated +1 V". Considering that the change in the photoelectron energy in this case is induced by the applied 1 V external potential, the "hydrated +1 V" spectrum was shifted by 1 eV towards lower BE for further spectral analysis. This calibration can be validated because the BE position of oxygen component in perovskite lattice at 528.9 eV is aligned at all the three conditions investigated, which will be discussed later. Comparing the O 1s spectra measured at three conditions in Figure 1(c), the two hydrated spectra exhibit two distinct peaks. For both hydrated spectra, the small peaks at higher binding energy (BE) (534-536 eV) are almost identical in shape. Given that in O 1s spectra, signal from H_2O at the surface of oxides locates at 535-536 eV[40, 41] and the dry spectrum shows no obvious signal in this region, we conclude that the small distinct peaks centered at about 534.5 eV in both hydrated spectra arise from water vapor immediately above the surface. There is an about 0.2 eV offset of this water vapor phase to lower BE side after applying potential. Since the position of gas phase peak is closely related to the surface work function,[42] this peak shift indicates the increase of surface work function. Since this peak does not provide information about oxygen in BZY, it is not discussed further below.

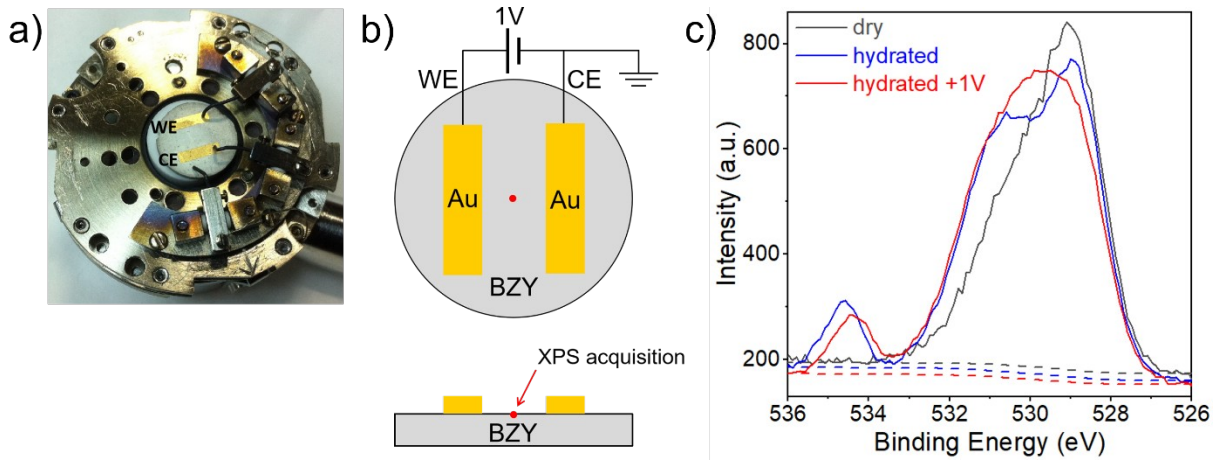

Figure 1. (a) BZY mounted on sample holder and (b) Schematic drawing of top and sectional view for the BZY pellet and electrical connection. WE: working electrode; CE: counter electrode (grounded). (c) O 1s spectra for BZY measured at ~550 K in subsequently changed conditions: UHV (dry, black), 200 mTorr water vapor (hydrated, blue), and then applying 1V external potential (hydrated +1V, red). Spectra were measured at photon energy of 700 eV.

The hydration process of the BZY is initiated by introducing water vapor into the chamber. In Figure 1(c), the overall intensity of the main peak (526-534 eV, excluding the small water vapor peak) in hydrated spectrum is 1.1-fold larger than that of the dry spectrum. The amount of oxygen from water vapor filling into the lattices is over the stoichiometric oxygen vacancy of 5% in BZY10, as a result of the thermal treatment in UHV before measurement. Notably, the increase in intensity is inhomogeneous over the entire region. Comparing to the dry spectrum, the hydrated spectrum shows more significant increase in intensity at higher BE between 530 eV and 534 eV and a slight decrease at about 529 eV. Applying 1 V potential to the hydrated BZY does not alter the overall peak intensity, yet, distinctly changes the peak shape. This redistribution of spectral weight may be attributed to the effect through hydration process.

Understanding the hydration mechanism is essential to optimize the performance for proton conducting electrolytes. A critical parameter governing the performance of electrolyte is the hydration level, which is related to the concentration of protons and oxygen vacancies.[3] Therefore, it is necessary to quantify the spectral differences caused by hydration.

In Figure 2, the 526~533.5 eV band in each O 1s spectrum is deconvoluted using four components, with fitting details provided in SI. The four components are considered as four contributions of oxygen with different chemical environment. The yellow peaks centered at 528.9 eV, are assigned to intrinsic oxygen in the perovskite lattice[29, 43] (denoted as "lattice O"). The green peaks at 530.4 eV are attributed to surface species of undercoordinated oxygen in the crystal terminal plane, namely not coordinated to two B site cations and more weakly bound than lattice O[44, 45] (denoted as "undercoordinated O"). This component is also considered by others to associate with partially hydrated surface secondary phases like yttrium hydroxide.[30] The violet peaks at 531.4 eV represent the hydroxyl groups caused by hydration, which also includes dissociative absorbed water, terminated and multi-coordinated hydroxyls[18, 31, 46, 47] (denoted as "-OH"). The blue peaks at 533.0 eV may come from the adsorbed intact H_2O on the surface.[27, 41] The intensity of this component is very small (lower than 1.5%) in all spectra, because there is only small amount of the adsorbed H_2O on the surface at the experiment temperature of 550 K. This component may also contain C-O induced by the carbon contamination, however, since this peak is very small in all spectra, we do not discuss further on it. Figure 2 shows the proportion of each component in this region (excluding the water vapor peak).

The dry BZY has the lowest contribution from -OH (9.6%) and the highest contribution from lattice O (61.5%). After introducing water vapor, -OH contribution increases to 18.7%,

indicating that hydration occur through the dissociation of H_2O molecules forming -OH. There are also dissociative adsorption of water at the surface oxygen sites to form hydroxyls.[18] Upon hydration, the increase of -OH is 9.1%, consistent with the 10% increase in the total intensity of O 1s peak after introducing water vapor. Therefore, we attribute this total intensity increase to the increase of -OH. The decrease of lattice O component from 61.5% to 48.4% can divide into two parts: one part of lattice oxygen form -OH bonds with hydrogen atoms; other lattice oxygen ions may be influenced by oxygen filling the surrounding vacancies through hydration and change to an undercoordinated state. Therefore, the hydration effect on BZY is two-fold: not only the formation of -OH, but also the increase of undercoordinated O.

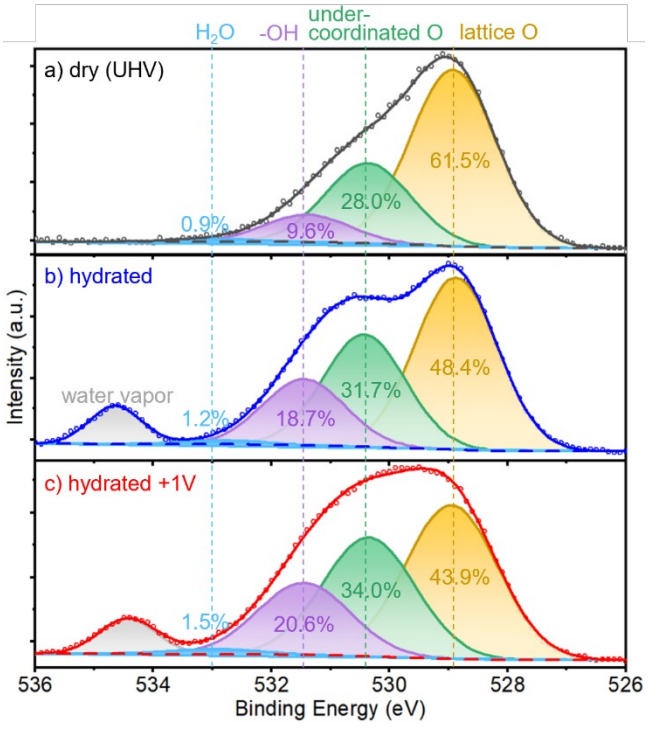

Figure 2. O 1s spectra for BZY at three conditions, deconvoluted by four peaks with same width and constrained position: lattice O (yellow, 528.9 eV); undercoordinated O (green, 530.4 eV); hydroxyl group -OH (violet, 531.4 eV); adsorbed intact H_2O (blue, 533.0 eV).

Applying 1 V potential to BZY further reinforces these changes with a slightly increase in -OH from 18.7% to 20.6%; meanwhile, a more remarkable enhancement appears in undercoordinated O, which increases from 31.7% to 34.0%, accompanied with the decrease in lattice O component. Major effect of potential is that the intrinsic lattice O are turned to undercoordinated state with higher activity. In this way, applying potential promotes hydration.

The core level XPS spectra of Ba 4d, Zr 3d and Y 3d are recorded at photon energy of 490 eV, as shown in Figure S3-5, and peak fitting details in Table S1-3. For the Ba 4d spectra, changes are trivial in the peak position under different conditions. Whereas for the Y 3d spectra, comparing to the dry spectrum, the hydrated spectrum shows a shift of about 0.1 eV toward lower BE. This phenomenon could be associated with a slight decrease in Y^{3+} oxidation state, implying that Y^{3+} is more reactive with water than Zr^{4+}. However, a shift of 0.2 and 0.1 eV toward higher BE can be found in both Y and Zr spectra with 1 V potential, respectively, which may result from the broadening of surface potential under applied bias. These changes in Zr and Y are relatively small comparing to the Ce and Y spectra in $BaCe_{1-x}Y_xO_{3-\delta}$ when varying the sample environment.[29,30,31] The changes in O 1s spectra among different conditions appear to be not relevant to other cations in the BZY lattice, as no significant changes are observed in XPS spectra of other elements. Note that the inelastic mean free path for O 1s core level XPS is about

8 Å at photon energy of 700 eV.[30] Therefore, the XPS analyses in this work are subject to the top surface layer in BZY.

Our analysis shows similar phenomenon as observed in photoelectrochemical water splitting on iron oxide.[48] In the presence of an electric field at the surface, the dipole moments of water molecules at the electrolyte-water interface are aligned. One possible interpretation for this observation is that the potential applied to the electrolyte tends to counteract the negative surface potential resulting from surface hydroxyl formation, and cause dielectric breakdown in surface water ordering, accompanied by a decrease in hydrogen bonding. The hydrogen bonds between water molecules may break, which may be in favor of water dissociated adsorption and formation of new hydroxyl bonds. Hence, the change of surface electric field by applied potential may result in enhanced hydration to BZY electrolyte surface. The underlying circumstances would be a matter of future work.

Impedance spectra were measured under the three successive conditions, as shown in the Nyquist plot in Figure 3(a). The equivalent circuit used for the spectra deconvolution is shown in the inset of Figure 3(a). The conductivities were calculated from impedance fitting details, as shown in Table S4.

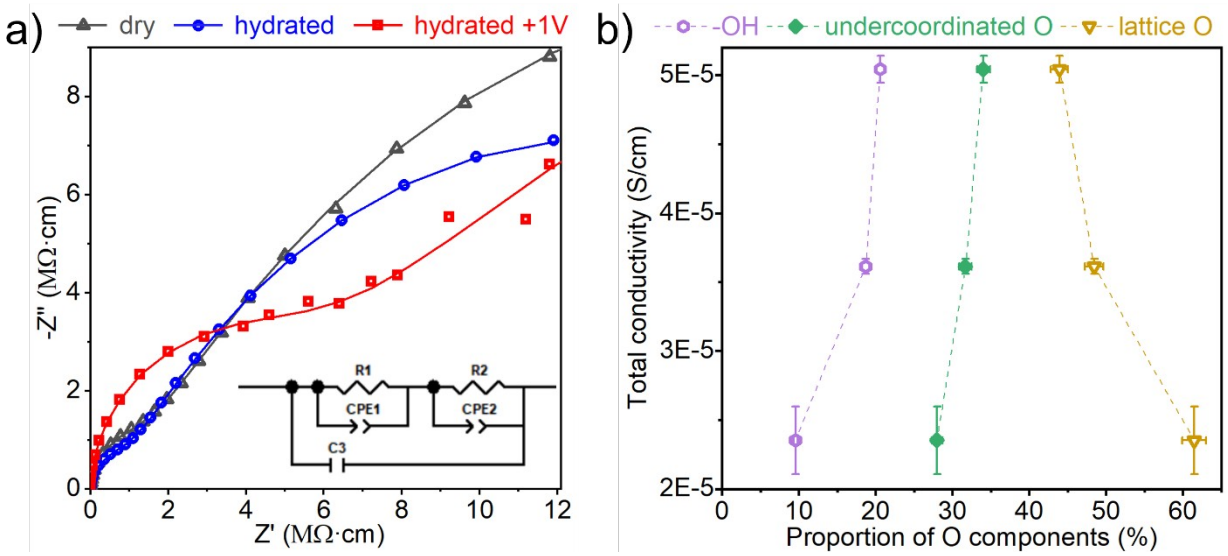

Figure 3. (a) Impedance Nyquist plots of BZY at high frequency at three conditions. Fitting equivalent circuit is shown in the inset. (b) Total conductivity of BZY versus the proportion of different oxygen components.

Here, we discuss the influence of potential on the proton conductivity from the viewpoint of chemical structure changes of surface oxygen. To demonstrate the hydration effect, in Figure 3(b), the total proton conductivities under the three conditions are shown as a function of the proportion change of the three spectral components in O 1s spectra. The proton conductivity increases from $2.3*10^{-5}$ S/cm at dry condition to $3.6*10^{-5}$ S/cm when hydrated. Upon hydration, hydroxyl protons form to increase charge carrier concentration, confirmed by the increase of -OH component. The undercoordinated O component also increases, resulting in an increase in the active sites for proton diffusion, thus facilitate protons hopping between adjacent oxygen sites and increase the proton mobility.

When applying 1V potential in hydrated condition, the proton conductivity further increases to $5.0*10^{-5}$ S/cm. This highest proton conductivity coincides with the most intense hydration effect (with the highest -OH, highest undercoordinated O and lowest lattice O contribution). In particular, after applying 1V potential, about 4.5% more lattice oxygen turns to -OH or undercoordinated state, providing more active sites for proton diffusion. Therefore, *in situ* NAP-XPS reveals the mechanism of enhanced surface hydration by applying potential, that positively impacts proton conductivity of BZY.

As the condition changed, there is no change in the apparent polarization resistance (horizontal axis intercept from impedance spectra), which is derived from the influence from ionic and electronic resistances.[49] Therefore, the conductivity improvement is predominantly contributed by protons but not electrons. Meanwhile, applying potential does not have an impact on this aspect.

Both the bulk and grain boundary conductivities are increased after hydration and applying potential. The improved proton conductivity is contributed by several complex effects. As proposed by Riess et al.[50], applying bias can lower the hopping barrier of a single particle transfer to the neighboring site, thus the proton transfer may be easier with potential. In addition, according to the space charge layer model, the applied potential decreases the effective barrier height and depletion layer of the mobile charge carriers, leading to a decrease in grain boundary resistance.[34]

Advisable improvements of working environment (such as raising temperature, increasing water content, providing oxidizing atmosphere) can increase the proton conductivity to various

degrees.[38, 51, 52] The effect of undercoordinated oxygen component may have been underestimated before. Moreover, this redistribution of O components could also be controlled by changing temperature or environmental atmosphere and so on.[30, 31] Hence, the chemical environment of O should be taken more seriously when studying proton conductor improvements. It is worth noting that XPS is a surface technique. As observed by Makagon et al.[53], doped $BaZrO_3$ exhibits non-classical electrostriction behavior, which means that under large electric field, the location of protons affects the elastic dipole moment in the lattice, imposing changes in the crystal structure. Other characterization methods, such as *in situ* X-Ray Diffraction or Raman spectroscopy, could be used under applied external potential to explore the behavior of protons in ceramics.

In this work, we use *in situ* NAP-XPS combined with impedance spectroscopy to investigate the effects of hydration on the chemical environment of surface oxygen and the conductivity of BZY proton conductor. As the operating conditions changed from dry to hydrated, we observe from O 1s spectra an enhancement in hydration, including 9.1% higher hydroxyl groups and 3.7% higher undercoordinated O component. Applying 1V potential further increases the hydroxyl groups by 1.9% and undercoordinated O by 2.3%, accompanied with conductivity improvement. We propose that applying 1V potential can enhance hydration on BZY surface. The proton conductivity can be improved by not only hydroxyl formation, but also the increased active proton sites at undercoordinated oxygen. The new chemical insights on hydration suggest a new approach to improve proton conductivity in ceramics by increasing the undercoordinated oxygen, which has potential significance for the development of protonic devices such as ceramic fuel cells and electrolyzers.

ASSOCIATED CONTENT

Supporting Information

The Supporting Information is available free of charge.

Materials and synthesis, impedance acquisition, in situ NAP-XPS characterization, XPS data analysis about O 1s, Ba 4d, Zr 3d and Y 3d (Figure S1-5, Table S1-3), impedance data analysis (Table S4) (PDF)

AUTHOR INFORMATION

Notes

The authors declare no competing financial interest.

ACKNOWLEDGMENTS

This work is supported by the National Natural Science Foundation of China Grant # 51802193, Swiss National Science Foundation Grant # 188588, 124812, SNF Swiss-Korea Collaboration Grant # IZK0Z2-133944, and Korea-Swiss Project SOPEM. Authors acknowledge valuable discussions with Truls Norby (University of Oslo). Sandia National Laboratories is a multimission laboratory managed and operated by National Technology and Engineering Solutions of Sandia LLC, a wholly owned subsidiary of Honeywell International Inc. for the U.S. Department of Energy's National Nuclear Security Administration under contract DE-NA0003525. This paper describes objective technical results and analysis. Any subjective views or opinions that might be expressed in the paper do not necessarily represent the views of the U.S. Department of Energy or the United States Government.

REFERENCES

(1) Duan, C.; Kee, R. J.; Zhu, H.; Karakaya, C.; Chen, Y.; Ricote, S.; Jarry, A.; Crumlin, E. J.; Hook, D.; Braun, R.; et al. Highly Durable, Coking and Sulfur Tolerant, Fuel-Flexible Protonic Ceramic Fuel Cells. *Nature* **2018**, *557* (7704), 217-222, DOI: 10.1038/s41586-018-0082-6

(2) Fabbri, E.; Pergolesi, D.; Traversa, E. Materials Challenges Toward Proton-Conducting Oxide Fuel Cells: A Critical Review. *Chem. Soc. Rev.* **2010**, *39* (11), 4355-4369, DOI: 10.1039/b902343g

(3) Kreuer, K. D. Proton-Conducting Oxides. *Annu. Rev. Mater. Res.* **2003**, *33*, 333-359, DOI: 10.1146/annurev.matsci.33.022802.091825

(4) Bi, L.; Da'as, E. H.; Shafi, S. P. Proton-Conducting Solid Oxide Fuel Cell (SOFC) with Y-Doped BaZrO3 Electrolyte. *Electrochem. Commun.* **2017**, *80*, 20-23, DOI: 10.1016/j.elecom.2017.05.006

(5) Vera, C. Y. R.; Ding, H. P.; Peterson, D.; Gibbons, W. T.; Zhou, M.; Ding, D. A Mini-Review on Proton Conduction of BaZrO3-Based Perovskite Electrolytes. *J. Phys-Energy* **2021**, *3* (3), 032019, DOI: 10.1088/2515-7655/ac12ab

(6) Stotz, S.; Wagner, C. Die Löslichkeit von Wasserdampf und Wasserstoff in festen Oxiden. *Ber. Bunsen-Ges. Phys. Chem.* **1966**, *70*, 781-788, DOI: 10.1002/bbpc.19660700804

(7) Uchida, H.; Maeda, N.; Iwahara, H. Relation Between Proton and Hole Conduction in SrCeO3-Based Solid Electrolytes under Water-Containing Atmospheres at High Temperatures. *Solid State Ion.* **1983**, *11* (2), 117-124, DOI: 10.1016/0167-2738(83)90048-6

(8) Nowick, A. S.; Yang, D. High-Temperature Protonic Conductors with Perovskite-Related Structures. *Solid State Ion.* **1995**, *77* (1), 137-146, DOI: 10.1016/0167-2738(94)00230-p

(9) Agmon, N. The Grotthuss mechanism. *Chem. Phys. Lett.* **1995**, *244* (5-6), 456-462, DOI: 10.1016/0009-2614(95)00905-j

(10) Agmon, N.; Bakker, H. J.; Campen, R. K.; Henchman, R. H.; Pohl, P.; Roke, S.; Thamer, M.; Hassanali, A. Protons and Hydroxide Ions in Aqueous Systems. *Chem. Rev.* **2016**, *116* (13), 7642-7672, DOI: 10.1021/acs.chemrev.5b00736

(11) Kreuer, K. D. Aspects of the Formation and Mobility of Protonic Charge Carriers and the Stability of Perovskite-Type Oxides. *Solid State Ion.* **1999**, *125* (1-4), 285-302, DOI: 10.1016/s0167-2738(99)00188-5

(12) Han, D.; Kishida, K.; Shinoda, K.; Inui, H.; Uda, T. A Comprehensive Understanding of Structure and Site Occupancy of Y in Y-doped BaZrO3. *J. Mater. Chem. A* **2013**, *1* (9), 3027-3033, DOI: 10.1039/c2ta00675h

(13) Pena, M. A.; Fierro, J. L. G. Chemical Structures and Performance of Perovskite Oxides. *Chem. Rev.* **2001**, *101* (7), 1981-2017, DOI: 10.1021/cr980129f

(14) Ricote, S.; Bonanos, N.; Caboche, G. Water Vapour Solubility and Conductivity Study of the Proton Conductor BaCe(0.9-x)ZrxY0.1O(3-delta). *Solid State Ion.* **2009**, *180* (14-16), 990-997, DOI: 10.1016/j.ssi.2009.03.016

(15) Yamazaki, Y.; Babilo, P.; Haile, S. M. Defect Chemistry of Yttrium-Doped Barium Zirconate: A Thermodynamic Analysis of Water Uptake. *Chem. Mater.* **2008**, *20* (20), 6352-6357, DOI: 10.1021/cm800843s

(16) Li, S.; Ma, R.; Pei, Y.; Mao, B.; Lu, H.; Yang, M.; Thomas, T.; Liu, D.; Wang, J. Geometric Structure and Electronic Polarization Synergistically Boost Hydrogen Evolution Kinetics in Alkaline Medium. *J. Phys. Chem. Lett.* **2020**, *11* (9), 3436-3442, DOI: 10.1021/acs.jpclett.0c00703

(17) Druce, J.; Tellez, H.; Burriel, M.; Sharp, M. D.; Fawcett, L. J.; Cook, S. N.; McPhail, D. S.; Ishihara, T.; Brongersma, H. H.; Kilner, J. A. Surface Termination and Subsurface Restructuring of Perovskite-Based Solid Oxide Electrode Materials. *Energy Environ. Sci.* **2014**, *7* (11), 3593-3599, DOI: 10.1039/c4ee01497a

(18) Stub, S. O.; Vollestad, E.; Norby, T. Mechanisms of Protonic Surface Transport in Porous Oxides: Example of YSZ. *J. Phys. Chem. C* **2017**, *121* (23), 12817-12825, DOI: 10.1021/acs.jpcc.7b03005

(19) Tande, C.; Perez-Coll, D.; Mather, G. C. Surface Proton Conductivity of Dense Nanocrystalline YSZ. *J. Mater. Chem.* **2012**, *22* (22), 11208-11213, DOI: 10.1039/c2jm31414b

(20) Yang, J.; Lu, Y.; Jin, L.; Zhao, C.; Chen, Y.; Xu, Y.; Chen, F.; Feng, J. Dynamic Optical Visualization of Proton Transport Pathways at Water–Solid Interfaces. *Angew. Chem. Int. Ed.* **2022**, *61* (2), e202112150, DOI: 10.1002/anie.202112150

(21) Warburton, R. E.; Mayer, J. M.; Hammes-Schiffer, S. Proton-Coupled Defects Impact O-H Bond Dissociation Free Energies on Metal Oxide Surfaces. *J. Phys. Chem. Lett.* **2021**, *12* (40), 9761-9767, DOI: 10.1021/acs.jpclett.1c02837

(22) Miyoshi, S.; Akao, Y.; Kuwata, N.; Kawamura, J.; Oyama, Y.; Yagi, T.; Yamaguchi, S. Low-Temperature Protonic Conduction Based on Surface Protonics: An Example of Nanostructured Yttria-Doped Zirconia. *Chem. Mater.* **2014**, *26* (18), 5194-5200, DOI: 10.1021/cm5012923

(23) Jing, Y.; Matsumoto, H.; Aluru, N. R. Mechanistic Insights into Hydration of Solid Oxides. *Chem. Mater.* **2018**, *30* (1), 138-144, DOI: 10.1021/acs.chemmater.7b03476

(24) Evarestov, R. A.; Bandura, A. V.; Alexandrov, V. E. Adsorption of Water on (001) Surface of SrTiO3 and SrZrO3 Cubic Perovskites: Hybrid HF-DFT LCAO Calculations. *Surf. Sci.* **2007**, *601* (8), 1844-1856, DOI: 10.1016/j.susc.2007.02.010

(25) Dawson, J. A.; Miller, J. A.; Tanaka, I. First-Principles Insight into the Hydration Ability and Proton Conduction of the Solid State Proton Conductor, Y and Sn Co-Doped BaZrO3. *Chem. Mater.* **2015**, *27* (3), 901-908, DOI: 10.1021/cm504110y

(26) Meyer, Q.; Zeng, Y.; Zhao, C. In Situ and Operando Characterization of Proton Exchange Membrane Fuel Cells. *Adv. Mater.* **2019**, *31* (40), 1901900, DOI: 10.1002/adma.201901900

(27) Arrigo, R.; Haevecker, M.; Schuster, M. E.; Ranjan, C.; Stotz, E.; Knop-Gericke, A.; Schloegl, R. In Situ Study of the Gas-Phase Electrolysis of Water on Platinum by NAP-XPS. *Angew. Chem. Int. Ed.* **2013**, *52* (44), 11660-11664, DOI: 10.1002/anie.201304765

(28) Feng, Z.; Crumlin, E. J.; Hong, W. T.; Lee, D.; Mutoro, E.; Biegalski, M. D.; Zhou, H.; Bluhm, H.; Christen, H. M.; Shao-Horn, Y. In Situ Studies of the Temperature-Dependent Surface Structure and Chemistry of Single-Crystalline (001)-Oriented La0.8Sr0.2CoO3-delta Perovskite Thin Films. *J. Phys. Chem. Lett.* **2013**, *4* (9), 1512-1518, DOI: 10.1021/jz400250t

(29) Chen, Q.; El Gabaly, F.; Akgul, F. A.; Liu, Z.; Mun, B. S.; Yamaguchi, S.; Braun, A. Observation of Oxygen Vacancy Filling under Water Vapor in Ceramic Proton Conductors in Situ with Ambient Pressure XPS. *Chem. Mater.* **2013**, *25* (23), 4690-4696, DOI: 10.1021/cm401977p

(30) Jarry, A.; Ricote, S.; Geller, A.; Pellegrinelli, C.; Zhang, X.; Stewart, D.; Takeuchi, I.; Wachsman, E.; Crumlin, E. J.; Eichhorn, B. Assessing Substitution Effects on Surface Chemistry by In Situ Ambient Pressure X-ray Photoelectron Spectroscopy on Perovskite Thin Films, BaCexZr0.9-xY0.1O2.95 (x=0; 0.2; 0.9). *ACS Appl. Mater. Interfaces* **2018**, *10* (43), 37661-37670, DOI: 10.1021/acsami.8b12546

(31) Jarry, A.; Jackson, G. S.; Crumlin, E. J.; Eichhorn, B.; Ricote, S. The Effect of Grain Size on the Hydration of BaZr0.9Y0.1O3-delta Proton Conductor Studied by Ambient Pressure X-ray Photoelectron Spectroscopy. *Phys. Chem. Chem. Phys.* **2020**, *22* (1), 136-143, DOI: 10.1039/c9cp04335g

(32) Chen, M.; Xie, X.; Guo, J.; Chen, D.; Xu, Q. Space Charge Layer Effect at the Platinum Anode/BaZr0.9Y0.1O3-delta Electrolyte Interface in Proton Ceramic Fuel Cells. *J. Mater. Chem. A* **2020**, *8* (25), 12566-12575, DOI: 10.1039/d0ta03339a

(33) Gan, Y.; Zhang, J.; Li, Y.; Li, S.; Xie, K.; Irvine, J. T. S. Composite Oxygen Electrode Based on LSCM for Steam Electrolysis in a Proton Conducting Solid Oxide Electrolyzer. *J. Electrochem. Soc.* **2012**, *159* (11), F763-F767, DOI: 10.1149/2.018212jes

(34) Iguchi, F.; Chen, C.-T.; Yugami, H.; Kim, S. Direct Evidence of Potential Barriers at Grain Boundaries in Y-doped BaZrO3 from DC-Bias Dependence Measurements. *J. Mater. Chem.* **2011**, *21* (41), 16517-16523, DOI: 10.1039/c1jm12685g

(35) Li, S.; Xie, K. Composite Oxygen Electrode Based on LSCF and BSCF for Steam Electrolysis in a Proton-Conducting Solid Oxide Electrolyzer. *J. Electrochem. Soc.* **2013**, *160* (2), F224-F233, DOI: 10.1149/2.027303jes

(36) Vovk, G.; Chen, X. H.; Mims, C. A. In Situ XPS Studies of Perovskite Oxide Surfaces under Electrochemical Polarization. *J. Phys. Chem. B* **2005**, *109* (6), 2445-2454, DOI: 10.1021/jp0486494

(37) Raevski, I. P.; Maksimov, S. M.; Fisenko, A. V.; Prosandeyev, S. A.; Osipenko, I. A.; Tarasenko, P. F. Study of Intrinsic Point Defects in Oxides of the Perovskite Family: II. Experiment. *J. Phys.: Condens. Matter* **1998**, *10* (36), 8015-8032, DOI: 10.1088/0953-8984/10/36/012

(38) Lei, L.; Zhang, J.; Yuan, Z.; Liu, J.; Ni, M.; Chen, F. Progress Report on Proton Conducting Solid Oxide Electrolysis Cells. *Adv. Funct. Mater.* **2019**, *29* (37), 1903805, DOI: 10.1002/adfm.201903805

(39) Tomkiewicz, M.; Fay, H. Photoelectrolysis of Water with Semiconductors. *Appl. Phys.* **1979**, *18* (1), 1-28, DOI: 10.1007/bf00935899

(40) Patel, D. I.; Shah, D.; Bahr, S.; Dietrich, P.; Meyer, M.; Thissen, A.; Linford, M. R. Water Vapor, by Near-Ambient Pressure XPS. *Surf. Sci. Spectra* **2019**, *26* (1), 014026, DOI: 10.1116/1.5111634

(41) Yamamoto, S.; Bluhm, H.; Andersson, K.; Ketteler, G.; Ogasawara, H.; Salmeron, M.; Nilsson, A. In Situ X-ray Photoelectron Spectroscopy Studies of Water on Metals and Oxides at Ambient Conditions. *J. Phys.: Condens. Matter* **2008**, *20* (18), 184025, DOI: 10.1088/0953-8984/20/18/184025

(42) Axnanda, S.; Scheele, M.; Crumlin, E.; Mao, B.; Chang, R.; Rani, S.; Faiz, M.; Wang, S.; Alivisatos, A. P.; Liu, Z. Direct Work Function Measurement by Gas Phase Photoelectron Spectroscopy and Its Application on PbS Nanoparticles. *Nano Lett.* **2013**, *13* (12), 6176-6182, DOI: 10.1021/nl403524a

(43) van der Heide, P. A. W. Systematic X-ray Photoelectron Spectroscopic Study of La1−xSrx-Based Perovskite-Type Oxides. *Surf. Interface Anal.* **2002**, *33* (5), 414-425, DOI: 10.1002/sia.1227

(44) Knapp, M.; Crihan, D.; Seitsonen, A. P.; Lundgren, E.; Resta, A.; Andersen, J. N.; Over, H. Complex Interaction of Hydrogen with the RuO2(110) Surface. *J. Phys. Chem. C* **2007**, *111* (14), 5363-5373, DOI: 10.1021/jp0667339

(45) Stoerzinger, K. A.; Hong, W. T.; Crumlin, E. J.; Bluhm, H.; Biegalski, M. D.; Shao-Horn, Y. Water Reactivity on the LaCoO3 (001) Surface: An Ambient Pressure X-ray Photoelectron Spectroscopy Study. *J. Phys. Chem. C* **2014**, *118* (34), 19733-19741, DOI: 10.1021/jp502970r

(46) Barr, T. L. An ESCA Study of the Termination of the Passivation of Elemental Metals. *J. Phys. Chem.* **1978**, *82* (16), 1801-1810, DOI: 10.1021/j100505a006

(47) Ketteler, G.; Yamamoto, S.; Bluhm, H.; Andersson, K.; Starr, D. E.; Ogletree, D. F.; Ogasawara, H.; Nilsson, A.; Salmeron, M. The Nature of Water Nucleation Sites on TiO2(110) Surfaces Revealed by Ambient Pressure X-ray Photoelectron Spectroscopy. *J. Phys. Chem. C* **2007**, *111* (23), 8278-8282, DOI: 10.1021/jp068606i

(48) Braun, A.; Hu, Y.; Boudoire, F.; Bora, D. K.; Sarma, D. D.; Graetzel, M.; Eggleston, C. M. The Electronic, Chemical and Electrocatalytic Processes and Intermediates on Iron Oxide

Surfaces During Photoelectrochemical Water Splitting. *Catal. Today* **2016**, *260*, 72-81, DOI: 10.1016/j.cattod.2015.07.024

(49) Huan, D.; Wang, W.; Xie, Y.; Shi, N.; Wan, Y.; Xia, C.; Peng, R.; Lu, Y. Investigation of Real Polarization Resistance for Electrode Performance in Proton-Conducting Electrolysis Cells. *J. Mater. Chem. A* **2018**, *6* (38), 18508-18517, DOI: 10.1039/c8ta06862c

(50) Riess, I.; Maier, J. Symmetrized General Hopping Current Equation. *Phys. Rev. Lett.* **2008**, *100* (20), 205901, DOI: 10.1103/PhysRevLett.100.205901

(51) Ricote, S.; Bonanos, N.; Wang, H. J.; Boukamp, B. A. Conductivity Study of Dense BaZr0.9Y0.1O(3-delta) Obtained by Spark Plasma Sintering. *Solid State Ion.* **2012**, *213*, 36-41, DOI: 10.1016/j.ssi.2011.02.011

(52) Viviani, M.; Buscaglia, M. T.; Nanni, P.; Parodi, R.; Gemme, G.; Dacca, A. XPS Investigation of Surface Properties of Ba(1-x)SrxTiO3 Powders Prepared by Low Temperature Aqueous Synthesis. *J. Eur. Ceram. Soc.* **1999**, *19* (6-7), 1047-1051, DOI: 10.1016/s0955-2219(98)00371-9

(53) Makagon, E.; Kraynis, O.; Merkle, R.; Maier, J.; Lubomirsky, I. Non-Classical Electrostriction in Hydrated Acceptor Doped BaZrO3: Proton Trapping and Dopant Size Effect. *Adv. Funct. Mater.* **2021**, *31* (50), 2104188, DOI: 10.1002/adfm.202104188